Reversible Decay of Oxygen Evolution Activity of Iridium Catalysts

Robert Tang-Kong,[a] Chrisopher E.D. Chidsey,[b] and Paul C. McIntyre*[a]

[a] *Department of Materials Science and Engineering, Stanford University, Stanford, CA, United States*

[b] *Department of Chemistry, Stanford University, Stanford, CA, United States*

[*] *Corresponding author: pcm1@stanford.edu*

Abstract

Iridium has long been recognized as one of the best oxygen evolution catalysts in terms of activity and stability over a wide range of pH. Despite exhibiting initially high activity for the oxygen evolution reaction (OER), a rapid and reversible activity decay is observed during continuous operation. The potential dependence of recovery of the activity is explored, and 0.0 V vs NHE is found to be an effective potential to recover the initial water oxidation performance. Iridium thin films on rotating disk electrodes are used to show that this OER activity decay is neither explained by progressive oxidation of the iridium nor by reduced mass transport to/from the electrode surface. Careful examination of the time dependence of the activity decay reveals that it is well described by a $t^{-1/4}$ functional dependence across multiple electrochemical cell geometries. Tafel behavior is analyzed by normal pulse voltammetry, suggesting that, after 10 minutes of activity decay, the catalyst exhibits a five-fold decrease in active site density while the mechanism of water oxidation is not altered. We hypothesize that this decay may result from a loss of active sites capable of forming the Ir(V)=O species, possibly via progressive cross-linking of iridium sites by bridging mu-oxides.

Keywords: Iridium, oxygen evolution, catalyst, activity decay, tafel behavior

I. Introduction

The platinum group metals are renowned for their resistance to corrosion. Iridium, in particular, has gained attention for its ability to efficiently catalyze the oxygen evolution reaction over a wide range of pH[1] while resisting dissolution even in aqua regia.[2] As one of the few catalysts for the oxygen evolution reaction (OER) that is stable in acidic media,[3] iridium and iridium-based complexes have been frequently studied.[4–8] Acid stability is important technologically, particularly for technologies utilizing proton-exchange membranes.[9] Although iridium is typically thought to be thermodynamically stable, recent reports by Cherevko[10,11] have shown iridium's dissolution rate in acidic media to be non-negligible. These works show that iridium experiences detectable transient dissolution at both the anodic and cathodic potentials. However, the reported results suggest no direct link between iridium dissolution and OER activity. While iridium oxide may not be entirely resistant to corrosion, its high activity for OER remains widely accepted.

Prior reports have, however, described activity decay in iridium OER catalysts. For systems with limited amounts of catalyst available, activity decay can be justifiably attributed to loss of iridium itself.[3,12] However even in cases where bulk iridium electrodes are used, activity decay can be observed. The first to report on this intrinsic activity decay were Gottesfeld and Shrinivasan[13], observing a 5-10x decay in activity for bulk iridium electrodes (50% activity decay over 10's of minutes) coated with a 250-nm thick electrochemically grown iridium oxide layer. Critically, this decay was not permanent, and could be reversed by a single scan back to 0.25V vs the normal hydrogen electrode (NHE). Based on this rejuvenation requirement and a lack of any observable change in the bulk oxide properties,

it was hypothesized that stabilization of an inactive oxide phase under sufficient anodic potential was to blame for the decay in OER activity. Frazer and Woods also reported similar "ageing" after holding an iridium electrode at 1.55V vs NHE, and were able to reverse the activity decay by sweeping to more reducing potentials.[14] While a few have reported on this activity decay more recently,[15,16] many works show evidence for similar phenomena without mentioning the decay process explicitly.[3,11,17,18] The studies that do explore the activity decay argue the activity decay is due to a transition to a less active but more stoichiometric anhydrous IrO_2 phase generated during the oxygen evolution reaction. The ability of reducing potentials to reverse this intrinsic activity decay is also confirmed in these works. In particular, Tan et al[15] show by chronoamperometry that the activity decayed to less than 30% of their original value over 3 hours. After holding the electrode at open circuit for 10 minutes and performing a cyclic voltammogram, the activity could be restored at times back to 80% of the original value, but would quickly decay in a manner similar to the first chronoamperometry test. To date, iridium containing compounds are still being investigated with the goal of achieving high OER activity over long time periods.[7,19,20] Investigations of the OER mechanism on iridium-based catalysts have been plentiful;[6,21–25] however, no thorough study of the dynamics of this reversible activity decay has been reported.

This work presents a detailed characterization of this transient activity decay, and establishes a reproducible approach for resetting the activity of the iridium catalyst. Careful electrochemical characterization with very thin films of iridium on a rotating disk electrode establishes that the OER activity decay is neither explained by progressive oxidation of the iridium nor reduced mass transport to or from the electrode. Analysis of the activity as a

function of potential before and after the activity decay suggests a similar rate limiting step, but with 5x fewer active sites after the activity decay. Better understanding this phenomenon will enable iridium catalyst systems to be utilized to their full capacity, and may help find approaches to minimize activity decay.

II. Results and Discussion

One example of iridium oxide activity decay during OER can be observed with a relatively simple set of measurements. An iridium foil was submerged in 1M H_2SO_4 and a cyclic voltammogram between +0.5 V and +1.6 V vs NHE was collected at 0.1 V/s. After many cycles, the potential was stepped from 0.5V vs NHE to a potential of 1.53V vs NHE where oxygen evolution takes place. Seconds after the step, the activity decays to far less than the activity observed at 1.53 V in the cyclic voltammogram (**Figure 1**). After returning briefly to 0.5V vs NHE, the second chronoamperometry does not continue where the first left off, but recovers partially before exhibiting a similar activity decay behavior.

A potential of 0.25 V vs NHE was previously cited[13] as a potential sufficient to recover the OER activity decay, but the potential dependence of the recovery has not been explored. **Figure 2a** shows two chronoamperometry experiments performed on an iridium foil after spending 1 second at either 1.2V or 0.2V vs NHE. The time evolution of these two experiments shows that a history of more reducing potentials results in higher activity during the OER step. To more carefully investigate this effect, cyclic step chronoamperometry was utilized. The potential was cyclically stepped between a lower potential to promote recovery and a higher potential for the OER, where activity decays. The input potential waveform is a square wave with a period of 10 seconds and duty cycle of 50%, and can be thought of as

a series of 5 second chronoamperometry experiments with 5 second rest periods in between. In the case where the lower potential is 1.2 V vs NHE (green in **Figure 2b**), the initial activity of each short chronoamperogram approaches that of the steady state chronoamperogram (black in **Figure 2b**). In contrast, stepping back to 0.03V vs NHE for 5 seconds is sufficient to restore the activity to nearly the same point in every short chronoamperometry experiment. This recovery effect is consistent over the 10 min test period and 60 cycles. **Figure 2c** shows the percent decay over the 10 min cyclic step chronoamperometry experiment, calculated from the final current density of first and last positive steps. This shows that 5 seconds at 0.0 V vs NHE is sufficient to fully recover the activity.

The rate of recovery of the OER activity as a function of rest time was probed by the same cyclic step chronoamperometry experiment, showing that stepping to 0.0 V vs NHE for just 1 second fully rejuvenates the iridium catalyst surface activity after 9 seconds of OER.

Inspired by the results in **Figure 2**, longer time intervals were studied. **Figure 3a** shows the reproducibility of 10-minute long OER chronoamperometry after holding the potential for 5 minutes at 0.0 V vs. NHE.

Several electrochemical processes could be responsible for the activity decay. Given the character of the decay over time, one potential explanation would be mass transfer-limited depletion of reactant or accumulation of product at the catalyst-electrolyte interface. The effect of one dimensional diffusion in the electrolyte is well known,[26,27] and is described by the Cottrell equation **(1)**. The factor a_c collects multiple physical parameters, such as the diffusion coefficient and reactant concentration.

$$i = a_c t^{-1/2} \quad \textbf{(1)}$$

The Cottrell equation provides poor fits to the measured chronoamperometry both with and without an added constant current term, but a different power law with a $t^{-1/4}$ dependence ($i = a_u t^{-1/4}$) fits the data well (**Figure 3b)**.

Diffusion limitations were further investigated using iridium-coated rotating disk electrodes (RDE). Iridium thin films of various thickness were deposited onto titanium disks by e-beam evaporation. Varying the rate of rotation varies the rate of electrolyte flow to the surface of the electrode, which alters the diffusion-limited current.[26] However, when these iridium-coated titanium disks were used to carry out the OER (**Figure 4a, b**), the rotation rate had no systematic effect on the observed activity decay. This confirms that limitations on product or reactant diffusion in the electrolyte do not contribute significantly to the observed activity decay. The CA data obtained with rotation (**Figure 4c, d**) are also fit well by the same $t^{-1/4}$ dependence used to fit the unrotated data (**Figure 3b)**.

Use of an e-beam evaporated iridium thin film of known thickness also allows for more accurate investigation of the extent of oxidation during the reaction by changing thickness of the iridium film. Qualitatively, the fact that activities are similar for both 2 nm and 20 nm thick films suggests that the decay process is not dependent on the amount of iridium. The $i = a_u t^{-1/4}$ functional dependence discussed previously is found to fit both the 2-nm and 20-nm data quite well, with only slight differences in the prefactor a_u.

The current measured during electrochemical characterization inevitably involves contributions from both the oxidation of iridium and the oxidation of water. Charge balance

calculations show that the charge passed during the first 600 seconds of chronoamperometry far surpasses that required to oxidize a 2 nm-thick iridium film from Ir(0) to Ir(4+). Assuming the current flowing at 10 min is entirely attributable to the OER, a transient charge of roughly 90 mC/cm^2 would have passed between t = 0 and 10 min, which is represented by the blue shaded regions in **Figure 4a** and **4b**. This is 10x more than the 9 mC/cm^2 needed to convert a 2 nm-thick layer of face-centered cubic Ir from Ir(0) to Ir(4+). Therefore, although a small fraction of the initial current that exceeds the steady state current can be attributed to the oxidation of the film, a declining rate of iridium oxidation cannot account for the majority of the activity decay.

Electrochemical characterization was used to probe the behavior of iridium OER catalysts while the activity decay is present. An iridium foil was held at a rest potential for 5 minutes. The potential was pulsed to more positive potentials in order to probe the potential dependence of the OER activity (**Figure 5**). The potential was then returned to the original rest potential for 10 seconds before repeating the procedure. Two rest potentials were used (0.0 V and 1.53V vs NHE) to probe the state before and after the activity decay occurs.

The observed activity is significantly lower when pulsed from 1.53 V vs NHE. In order to examine the potential dependence of the activity following the steps from the two different rest potentials, the results are fit to the Tafel equation modified to account for the series resistance of the cell **(Equation (**2**).** The series resistance (R_s = 1.79 Ω·cm^2) was taken to be the real component of the high frequency impedance determined by electrochemical impedance spectroscopy. The standard redox potential for the oxygen evolution reaction (E_0) was fixed at 1.23 V vs NHE. The activity during each pulse was recorded after 1 millisecond

156 of polarization to allow time for the double layer charging current to decay (the decay time
157 was determined to be of the order of 35 μs by electrochemical impedance spectroscopy).

$$i = i_0 exp\left(\frac{\alpha F}{R_g T}(E - E_0 - iR_s)\right) \quad \textbf{(2)}$$

158 Fixing only the series resistance, R_s, and the reversible oxygen evolution potential, E_0,
159 yielded values for the charge transfer coefficient (α) of between 1 and 1.2. For simplicity,
160 fits were repeated with α set to 1, yielding adequate fits to the data **(Figure 5b and Table 1)**.
161 An α value of 1 suggests a rate determining chemical step following a single electron
162 transfer.[30] The difference between the extracted voltammograms is a five-fold decrease in
163 the exchange current density. The fact that similar charge transfer coefficients (α) can fit both
164 sets of data suggests that the reaction mechanism is not changing significantly, and that the
165 decrease in exchange current density can be interpreted as a loss in the number of active
166 catalytic sites.
167 It is interesting to note that both normal pulse voltammograms deviate significantly from the
168 continuously swept voltammogram also included in Figure 5b. The later time points in the
169 linear sweep voltammogram experience the progressive history of activity decay from earlier
170 in the sweep whereas such progressive history effects are absent in the normal pulse
171 voltammograms. The Tafel fits to the linear sweep voltammogram (not shown) yield values
172 of α close to those reported in the literature (roughly α = 0.82).[31] This suggests that
173 previously observed Tafel parameters have been convoluted with the decay of catalyst
174 activity.

The suggested chemical rate determining step following a single electron transfer is consistent with a catalytic cycle involving water nucleophilic attack on a terminal metal oxo site, a pathway for OER frequently proposed in the literature.[7,32] That pathway would involve the one electron oxidation of some Ir(IV) site to form an Ir(V)=O terminal metal oxo species, which reacts with water to form an O-O bond. One simple interpretation of the loss of active sites suggested by **Table 1** is a loss of sites capable of forming the Ir(V)=O species, which could be explained by progressive cross linking of iridium sites by bridging μ-oxides. This configuration would result in a loss of terminal oxo groups, preventing the water nucleophilic attack required to generate molecular oxygen. Nearby basic ligands properly positioned adjacent to terminal metal oxo sites in some molecular complexes have been found to assist in the removal of protons from the attacking water,[33,34] and recent work has also shown the ability of nearby metal atoms to enhance the activity of iridium catalysts.[35] These reports suggest that surface modification, particularly by way of mixed metal oxides and hydroxides may provide promising methods for enhancing or maintaining the activity of these active sites.

III. Conclusion

In this work a rapid and reversible decay in the OER activity of an iridium metal catalyst is explored. Cyclic step chronoamperometry experiments demonstrate that 0.0 V vs NHE for 1 second is sufficient to repeatably reverse the decay over many cycles. Reproducibility is established for chronoamperometry experiments out to 10 minutes. A limitation of product diffusion in the electrolyte is ruled out as the cause of the observed OER activity decay. A

196 $t^{-1/4}$ functional dependence is found to fit the decay process across the electrochemical cell
197 geometries investigated. Tafel modeling demonstrates that a five-fold reduction in the
198 exchange current density over 2 second to 10^2 seconds time scales is characteristic of the
199 iridium oxide after the activity decay, while the OER mechanism remains the same as for the
200 material after its activity has recovered. This study helps provide a basis for future
201 investigations of iridium-based catalysts aimed at identifying the underlying mechanism of
202 this OER activity decay and mitigating it, ultimately leading to more stable, high-
203 performance OER catalysts.

204 IV. Experimental Methods

205 *Iridium Metal Foil:* Iridium metal foil was supplied from Goodfellow, with purity 99.9% and
206 thickness 0.25 mm was used for various electrochemical measurements. Working area
207 during OER was 3.2 cm^2. Between experimental sessions, the foil was annealed in forming
208 gas at 450°C for 30min to fully reduce any residual oxide built up during previous
209 experiments. The foil was macroscopically rough and its composition verified to be pure by
210 X-ray photoelectron spectroscopy (XPS).

211 *Silicon substrates:* Heavily boron-doped (100) p-type silicon wafers (ρ = 0.001-0.002 Ω-cm,
212 thickness 500μm) were used as conductive silicon substrates for electrochemical
213 measurements. The 4" diameter wafers were used as received with a 1.5-2nm vendor
214 chemical oxide layer, as confirmed through ellipsometry. Samples for adhesion experiments
215 were fabricated on similar wafers (3" diameter, ρ = 0.001-0.005 Ω-cm, thickness 355-
216 405μm), and also used as received with a 1.5-2nm vendor chemical oxide layer.

Back contact and catalyst deposition. TiO_2 was deposited onto the as-received silicon substrates by ALD. 20 nm Pt back contacts and 2nm Ir catalyst layers were deposited by e-beam evaporation following ALD.

Atomic Layer Deposition (ALD): All TiO_2 films were deposited by ALD in a custom built reactor. Tetrakisdimethylamido titanium (TDMAT) was used as the titanium source and water vapor as the oxygen source. The silicon substrates were held at 170°C during the entire deposition. The chamber details are described elsewhere[36].

Electrochemical Characterization: All electrochemical measurements were made using a bored (5 mm diameter, 0.196cm^2 area) Teflon cone cell pressed against the front side of the anode to contain electrolyte and define the electrode area. A reference electrode (Ag(s) | AgCl(s) sat. KCl) and counter electrode (Pt wire, 1mm diameter) were used, and all potentials measured using either a Biologic or WaveNow potentiostat at room temperature. Cyclic Voltammograms were recorded at a scan rate of 100mV s^{-1}. Stability measurements were performed using a peristaltic pump to circulate solution at 1mL s^{-1}.

Acknowledgements

We thank T. Carver for metal e-beam evaporations. R.T. would also like to thank C. Hitzman and J. Jamtgaard of Stanford Nano Shared Facilities for guidance with XPS, AES, and SIMS. Part of this work was performed at the Stanford Nano Shared Facilities (SNSF), supported by the National Science Foundation under award ECCS-1542152. This work was partially supported by National Science Foundation programs CBET-1805084, CBET-1336844, and the Stanford Institute for Materials & Energy Sciences.

References

(1) Pourbaix, M. *Atlas of Electrochemical Equilibria in Aqueous Solutions*, 1st ed.; Oxford, Pergamon Press: New York, 1966.

(2) Lyon, S. B. 3 . 21 Corrosion of Noble Metals. *Shreir's Corros.* **2010**, *1*, 3–6. https://doi.org/http://dx.doi.org/10.1016/B978-044452787-5.00109-8.

(3) McCrory, C. C. L.; Jung, S.; Peters, J. C.; Jaramillo, T. F. Benchmarking Heterogeneous Electrocatalysts for the Oxygen Evolution Reaction. *J. Am. Chem. Soc.* **2013**, *135* (45), 16977–16987. https://doi.org/10.1021/ja407115p.

(4) Reier, T.; Oezaslan, M.; Strasser, P. Electrocatalytic Oxygen Evolution Reaction (OER) on Ru, Ir, and Pt Catalysts: A Comparative Study of Nanoparticles and Bulk Materials. *ACS Catal.* **2012**, *2* (8), 1765–1772. https://doi.org/10.1021/cs3003098.

(5) Trasatti, S. Electrocatalysis in the Anodic Evolution of Oxygen and Chlorine. *Electrochim. Acta* **1984**, *29* (11), 1503–1512. https://doi.org/10.1016/0013-4686(84)85004-5.

(6) Fierro, S.; Nagel, T.; Baltruschat, H.; Comninellis, C. Investigation of the Oxygen Evolution Reaction on Ti/IrO2 Electrodes Using Isotope Labelling and on-Line Mass Spectrometry. *Electrochem. commun.* **2007**, *9* (8), 1969–1974. https://doi.org/10.1016/j.elecom.2007.05.008.

(7) Thomsen, J. M.; Huang, D. L.; Crabtree, R. H.; Brudvig, G. W. Iridium-Based Complexes for Water Oxidation. *Dalt. Trans.* **2015**, *44* (28), 12452–12472. https://doi.org/10.1039/C5DT00863H.

(8) Blakemore, J. D.; Mara, M. W.; Kushner-Lenhoff, M. N.; Schley, N. D.; Konezny,

S. J.; Rivalta, I.; Negre, C. F. A.; Snoeberger, R. C.; Kokhan, O.; Huang, J.; et al. Characterization of an Amorphous Iridium Water-Oxidation Catalyst Electrodeposited from Organometallic Precursors. *Inorg. Chem.* **2013**, *52* (4), 1860–1871. https://doi.org/10.1021/ic301968j.

(9) Carmo, M.; Fritz, D. L.; Mergel, J.; Stolten, D. A Comprehensive Review on PEM Water Electrolysis. *Int. J. Hydrogen Energy* **2013**, *38* (12), 4901–4934. https://doi.org/10.1016/j.ijhydene.2013.01.151.

(10) Cherevko, S.; Geiger, S.; Kasian, O.; Mingers, A.; Mayrhofer, K. J. J. Oxygen Evolution Activity and Stability of Iridium in Acidic Media. Part 1. - Metallic Iridium. *J. Electroanal. Chem.* **2016**, *773*, 69–78. https://doi.org/10.1016/j.jelechem.2016.04.033.

(11) Cherevko, S.; Geiger, S.; Kasian, O.; Mingers, A.; Mayrhofer, K. J. J. Oxygen Evolution Activity and Stability of Iridium in Acidic Media. Part 2. - Electrochemically Grown Hydrous Iridium Oxide. *J. Electroanal. Chem.* **2016**, *774*, 102–110. https://doi.org/10.1016/j.jelechem.2016.05.015.

(12) Tang-Kong, R.; Winter, R.; Brock, R.; Tracy, J.; Eizenberg, M.; Dauskardt, R. H.; McIntyre, P. C. The Role of Catalyst Adhesion in ALD-TiO $_2$ Protection of Water Splitting Silicon Anodes. *ACS Appl. Mater. Interfaces* **2018**, *10*, acsami.8b13576. https://doi.org/10.1021/acsami.8b13576.

(13) Gottesfeld, S.; Srinivasan, S. Electrochemical and Optical Studies of Thick Oxide Layers on Iridium and Their Electrocatalytic Activities for the Oxygen Evolution Reaction. *J. Electroanal. Chem. Interfacial Electrochem.* **1978**, *86* (1), 89–104.

https://doi.org/10.1016/S0022-0728(78)80358-1.

(14) Frazer, E. J.; Woods, R. The Oxygen Evolution Reaction on Cycled Iridium Electrodes. *J. Electroanal. Chem. Interfacial Electrochem.* **1979**, *102* (1), 127–130. https://doi.org/10.1016/S0022-0728(79)80036-4.

(15) Tan, X.; Shen, J.; Semagina, N.; Secanell, M. Decoupling Structure-Sensitive Deactivation Mechanisms of Ir/IrO x Electrocatalysts toward Oxygen Evolution Reaction. *J. Catal.* **2019**, *371*, 57–70. https://doi.org/10.1016/j.jcat.2019.01.018.

(16) Li, T.; Kasian, O.; Cherevko, S.; Zhang, S.; Geiger, S.; Scheu, C.; Felfer, P.; Raabe, D.; Gault, B.; Mayrhofer, K. J. J. Atomic-Scale Insights into Surface Species of Electrocatalysts in Three Dimensions. *Nat. Catal.* **2018**, *1* (4), 300–305. https://doi.org/10.1038/s41929-018-0043-3.

(17) Mei, B.; Pedersen, T.; Malacrida, P.; Bae, D.; Frydendal, R.; Hansen, O.; Vesborg, P. C. K.; Seger, B.; Chorkendorff, I. Crystalline TiO 2 : A Generic and Effective Electron Conducting Protection Layer for Photo-Anodes and -Cathodes. *J. Phys. Chem. C* **2015**, 150605155318000. https://doi.org/10.1021/acs.jpcc.5b04407.

(18) Satterthwaite, P. F.; Scheuermann, A. G.; Hurley, P. K.; Chidsey, C. E. D.; McIntyre, P. C. Engineering Interfacial Silicon Dioxide for Improved MIS Silicon Photoanode Water Splitting Performance. *ACS Appl. Mater. Interfaces* **2016**, acsami.6b03029. https://doi.org/10.1021/acsami.6b03029.

(19) Diaz-Morales, O.; Raaijman, S.; Kortlever, R.; Kooyman, P. J.; Wezendonk, T.; Gascon, J.; Fu, W. T.; Koper, M. T. M. Iridium-Based Double Perovskites for Efficient Water Oxidation in Acid Media. *Nat. Commun.* **2016**, *7*.

https://doi.org/10.1038/ncomms12363.

(20) Menendez Rodriguez, G.; Gatto, G.; Zuccaccia, C.; Macchioni, A. Benchmarking Water Oxidation Catalysts Based on Iridium Complexes: Clues and Doubts on the Nature of Active Species. *ChemSusChem* **2017**, *10* (22), 4503–4509. https://doi.org/10.1002/cssc.201701818.

(21) Sanchez Casalongue, H. G.; Ng, M. L.; Kaya, S.; Friebel, D.; Ogasawara, H.; Nilsson, A. In Situ Observation of Surface Species on Iridium Oxide Nanoparticles during the Oxygen Evolution Reaction. *Angew. Chem. Int. Ed. Engl.* **2014**, *53* (28), 7169–7172. https://doi.org/10.1002/anie.201402311.

(22) Pfeifer, V.; Jones, T. E.; Velasco Vélez, J. J.; Arrigo, R.; Piccinin, S.; Hävecker, M.; Knop-Gericke, A.; Schlögl, R. In Situ Observation of Reactive Oxygen Species Forming on Oxygen-Evolving Iridium Surfaces. *Chem. Sci.* **2017**, 2143–2149. https://doi.org/10.1039/C6SC04622C.

(23) Pfeifer, V.; Jones, T. E.; Knop-Gericke, A.; Schogl, R. The Electronic Structure of Iridium Oxide Electrodes Active in Water Splitting. *Phys. Chem. Chem. Phys.* **2016**, *18*, 2292–2296. https://doi.org/10.1039/C5CP06997A.

(24) Lyons, M. E. G.; Floquet, S. Mechanism of Oxygen Reactions at Porous Oxide Electrodes. Part 2—Oxygen Evolution at RuO2, IrO2 and IrxRu1−xO2 Electrodes in Aqueous Acid and Alkaline Solution. *Phys. Chem. Chem. Phys.* **2011**, *13* (12), 5314. https://doi.org/10.1039/c0cp02875d.

(25) Minguzzi, A.; Lugaresi, O.; Achilli, E.; Locatelli, C.; Vertova, A.; Ghigna, P.; Rondinini, S. Observing the Oxidation State Turnover in Heterogeneous Iridium-

Based Water Oxidation Catalysts. *Chem. Sci.* **2014**, *5*. https://doi.org/10.1039/C4SC00975D.

(26) Bard, A. J.; Faulkner, L. R. *Electrochemical Methods: Fundamentals and Applications*, 2nd ed.; Wiley: New York, 2000.

(27) Ribeiro, M. C.; Rego, L. G. C.; D'Ajello, P. C. T. Diffusion, Reaction and Forced Convection in Electrochemical Cells. *J. Electroanal. Chem.* **2009**, *628* (1–2), 21–26. https://doi.org/10.1016/j.jelechem.2008.12.018.

(28) Jadhav, S.; Meir, a J.; Bakker, E. Normal Pulse Voltammetry as Improved Pseudo Voltammetric Mode for Solvent Polymeric Ion Sensors. *Electroanalysis* **2000**, *12*, 1251–1257.

(29) Christie, J. H.; Parry, E. P.; Osteryoung, R. A. The Use of Normal Pulse Polarography in the Study of Electrode Kinetics. *Electrochim. Acta* **1966**, *11* (10), 1525–1529. https://doi.org/10.1016/0013-4686(66)80068-3.

(30) Shinagawa, T.; Garcia-Esparza, A. T.; Takanabe, K. Insight on Tafel Slopes from a Microkinetic Analysis of Aqueous Electrocatalysis for Energy Conversion. *Sci. Rep.* **2015**, *5* (September), 1–21. https://doi.org/10.1038/srep13801.

(31) Miles, M. H.; Klaus, E. A.; Gunn, B. P.; Locker, J. R.; Serafin, W. E.; Srinivasan, S. The Oxygen Evolution Reaction on Platinum, Iridium, Ruthenium and Their Alloys at 80°C in Acid Solutions. *Electrochim. Acta* **1978**, *23* (6), 521–526. https://doi.org/10.1016/0013-4686(78)85030-0.

(32) Blakemore, J. D.; Crabtree, R. H.; Brudvig, G. W. Molecular Catalysts for Water Oxidation. *Chem. Rev.* **2015**, *115* (23), 12974–13005.

https://doi.org/10.1021/acs.chemrev.5b00122.

(33) Vilella, L.; Vidossich, P.; Balcells, D.; Lledos, A. Basic Ancillary Ligands Promote O – O Bond Formation in Iridium-Catalyzed Water Oxidation : A DFT Study. *Dalt. Trans.* **2011**, *40*, 11241–11247. https://doi.org/10.1039/C1DT10660K.

(34) Matheu, R.; Ertem, M. Z.; Gimbert-Suriñach, C.; Benet-Buchholz, J.; Sala, X.; Llobet, A. Hydrogen Bonding Rescues Overpotential in Seven-Coordinated Ru Water Oxidation Catalysts. *ACS Catal.* **2017**, *7* (10), 6525–6532. https://doi.org/10.1021/acscatal.7b01860.

(35) Finke, C. E.; Omelchenko, S. T.; Jasper, J. T.; Lichterman, M. F.; Read, C. G.; Lewis, N. S.; Hoffmann, M. R. Enhancing the Activity of Oxygen-Evolution and Chlorine-Evolution Electrocatalysts by Atomic Layer Deposition of TiO 2. *Energy Environ. Sci.* **2019**. https://doi.org/10.1039/C8EE02351D.

(36) Scheuermann, A. G.; Lawrence, J. P.; Gunji, M.; Chidsey, C. E. D.; McIntyre, P. C. ALD-TiO 2 Preparation and Characterization for Metal-Insulator-Silicon Photoelectrochemical Applications. *Electrochem. Soc. Trans.* **2013**, *58* (10), 75–86. https://doi.org/10.1149/05810.0075ecst.

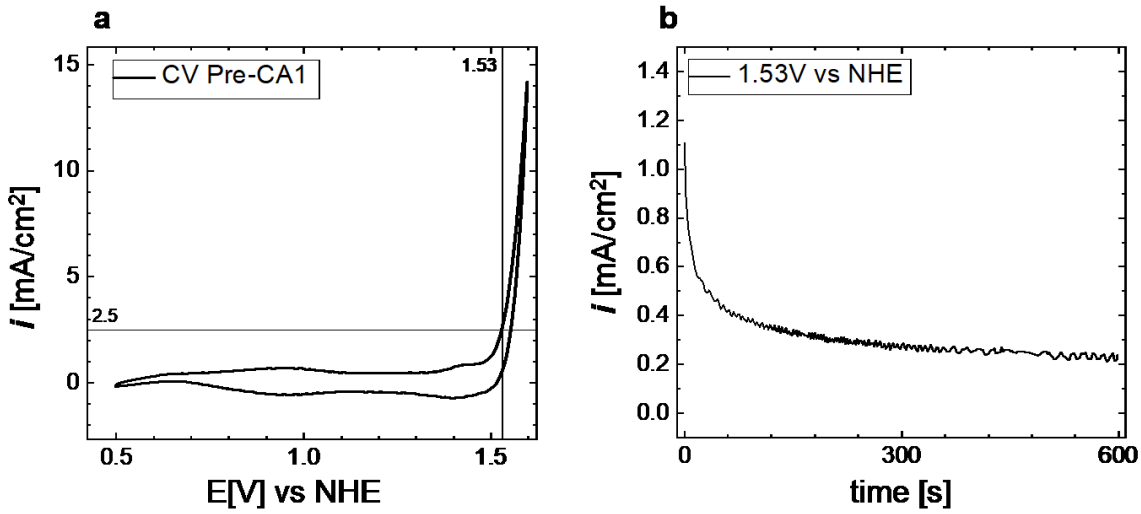

366

367 **Figure 1:** Electrochemical characterization of OER activity of an iridium metal foil in 1M H_2SO_4(aq)
368 electrolyte. Cyclic voltammograms (a) were taken immediately before the potential-step
369 chronoamperometry (b). Chronoamperometry was performed at 1.53V vs NHE after opening the
370 circuit at 0.5V vs NHE. The activity during chronoamperometry clearly decays below the level
371 expected given the cyclic voltammetry data for the same anode. This decay still occurs after holding
372 the potential at lower values.

373

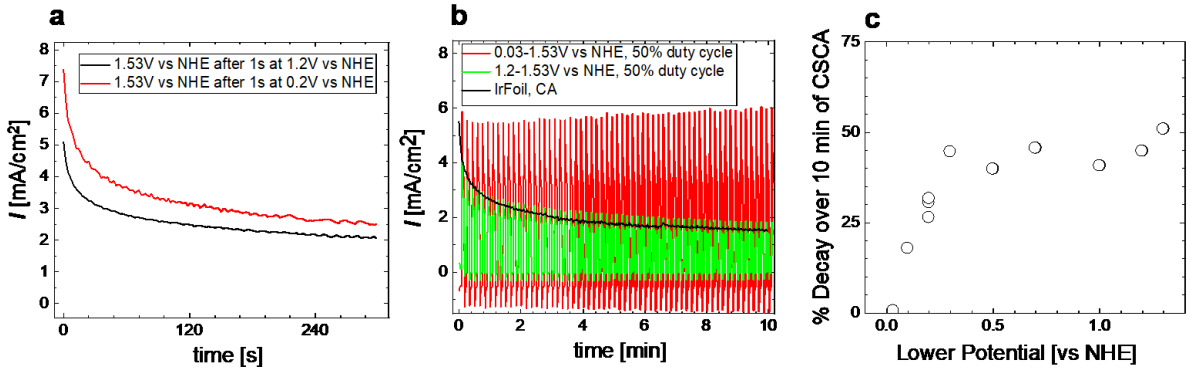

374

375 **Figure 2:** Investigation of the potential dependence of activity recovery. Experiments were
376 performed on an iridium foil in 1M H_2SO_4 in water. Panel (a) shows chronoamperometry experiments
377 after 1s at 1.2V or 0.2V vs NHE. Example cyclic step chronoamperometry is shown in panel (b) with
378 an upper potential of 1.53 V vs NHE and variable lower potential. During cyclic step
379 chronoamperometry the anode was cycled between an upper and lower potential, spending 5 seconds
380 at each potential. Insufficiently reducing lower potentials result in less water-oxidation activity
381 during subsequent upper potential steps. The results of varying the lower potential in the applied
382 waveform are shown in panel (c). A cyclic voltammogram from 0.5 V to 1.6 V vs NHE and back to
383 0.5 V at a scan rate of 0.1 V/s was performed between cyclic step chronoamperometry experiments
384 with different rest potentials.

385

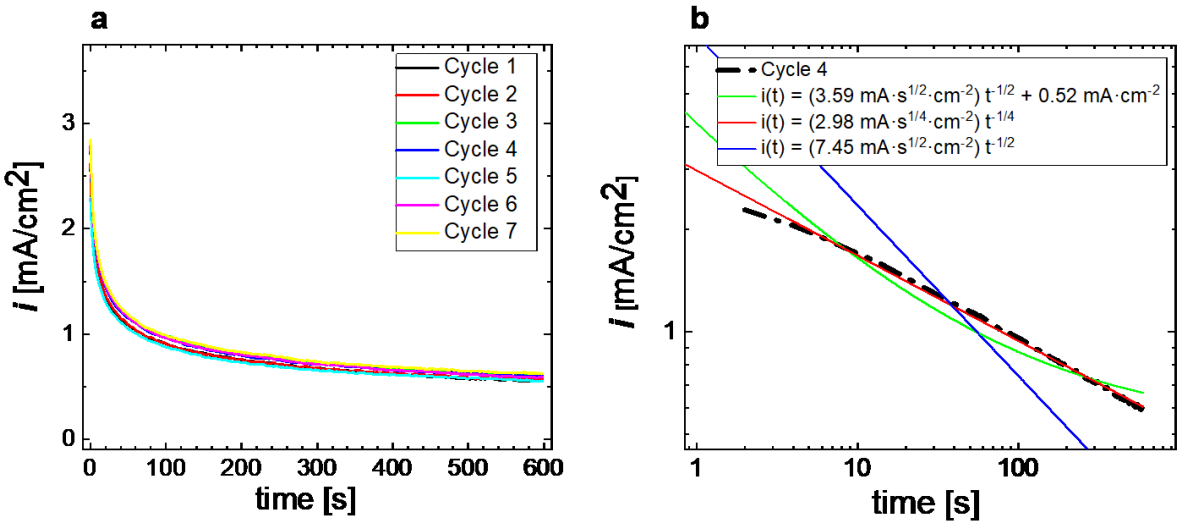

386

387 **Figure 3:** Chronoamperometry experiments demonstrating the reproducibility of the activity decay
388 behavior after using an electrochemical reset procedure between each successive CA test.
389 Experiments were performed on an iridium metal foil submersed in 1M H_2SO_4(aq) electrolyte. (a)
390 Repeated OER experiments, each performed after 5 min at 0.0 V vs NHE. (b) Comparison of three
391 different fits of a characteristic chronoamperometry experiment. A power law with an unusual
392 exponent of -1/4 and zero asymptote ($\boldsymbol{i = a_u t^{-1/4}}$) fits the data better than either the Cottrell equation
393 ($\boldsymbol{i = a_c t^{-1/2}}$) or a modified Cottrell equation with non-zero asymptote ($\boldsymbol{i = a_m t^{-1/2} + b}$)

394

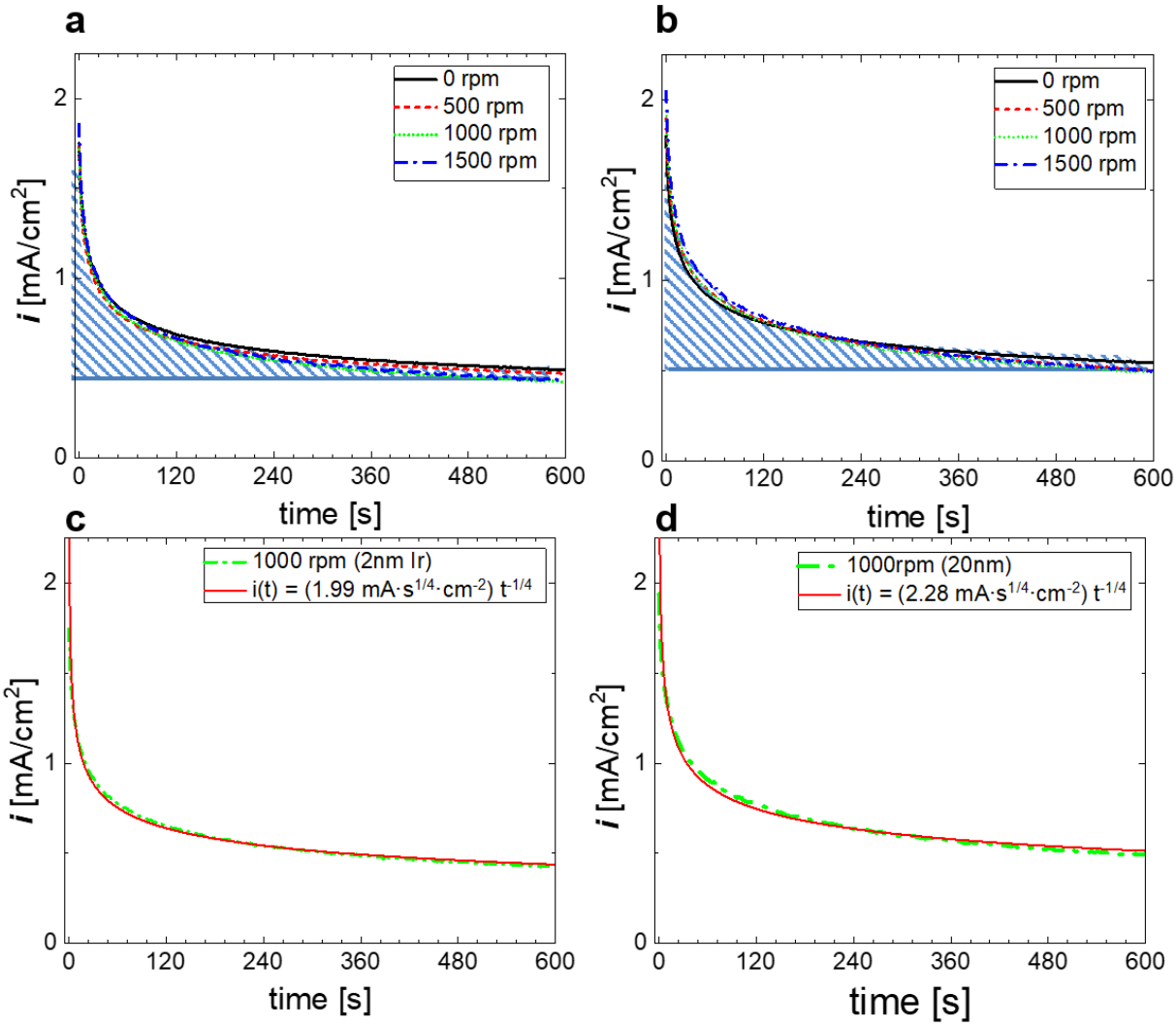

Figure 4: OER chronoamperometry on a **(**Ti Disk / 5 nm Ti / 2 or 20 nm Ir) electrode at various rotation rates. Chronoamperometry results for (a) a 2 nm Ir film and (b) a 20 nm Ir film at 1.53 V vs NHE, displaying nearly identical decay behavior regardless of rotation rate or film thickness. Shaded blue regions represent the transient charge passed if the current density measured at 600 seconds represented steady-state OER. $t^{-1/4}$ fits to the 2nm thick Ir (a) and 20 nm Ir (b) at 1000 rpm. A single cyclic voltammogram (0.7 V to 1.6 V and back to 0.7 V vs NHE at 0.1 V/s) was performed prior to each chronoamperogram.

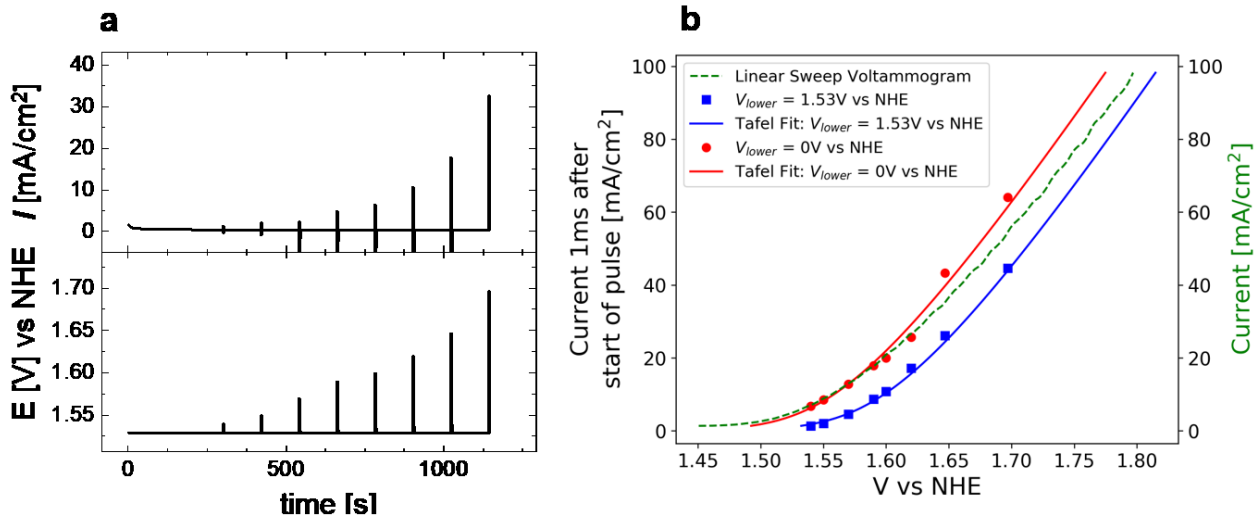

403

404 **Figure 5:** Normal pulse voltammetry experiment (a) and extracted voltammograms (blue and red
405 symbols) compared to a linear sweep voltammogram (b) on an iridium foil in 1M H_2SO_4(aq)
406 electrolyte. The linear sweep voltammogram (green dotted line) was collected at 0.1 V/s. Five
407 minutes of electrochemical reset, as described in the previous text, was performed prior to each
408 normal pulse voltammetry experiment. Tafel fits are for α set to 1.

409

Table 1: Fitted Tafel parameters for both the linear sweep voltammogram and pulsed voltammogram. Reversible oxygen evolution potential (E_0) and series resistance (R_s) were held constant at 1.23V vs NHE and 1.79 $\Omega \cdot cm^2$ respectively. The charge transfer coefficient (α) was fixed at 1. Exchange current density (i_0) was the only free variables used to fit **(2)**.

Resting Potential / V vs NHE	**i_0 / mA/cm^2**
0	5.72×10^{-5}
1.53	1.19×10^{-5}